Synthesis, Characterization, and Effects of Molecular Structure on Phase Behavior of 4-Chloro-1,3-Diazobenzene Bent-Core Liquid Crystals with High Photosensitivity

Jinying Lu[b], Daoren Yan[b], Zhiyong Zhang[a]*, and Zelong Zhang[b*]

[a]Department of Chemistry and Environmental Engineering, Wuhan Polytechnic University, Wuhan, China

[b]Department of Geology and Geophysics, Louisiana State University, Baton Rouge, LA, USA

Corresponding authors*

Zhiyong Zhang zzy6211@whpu.edu.cn

Zelong Zhang zelongz@lsu.edu

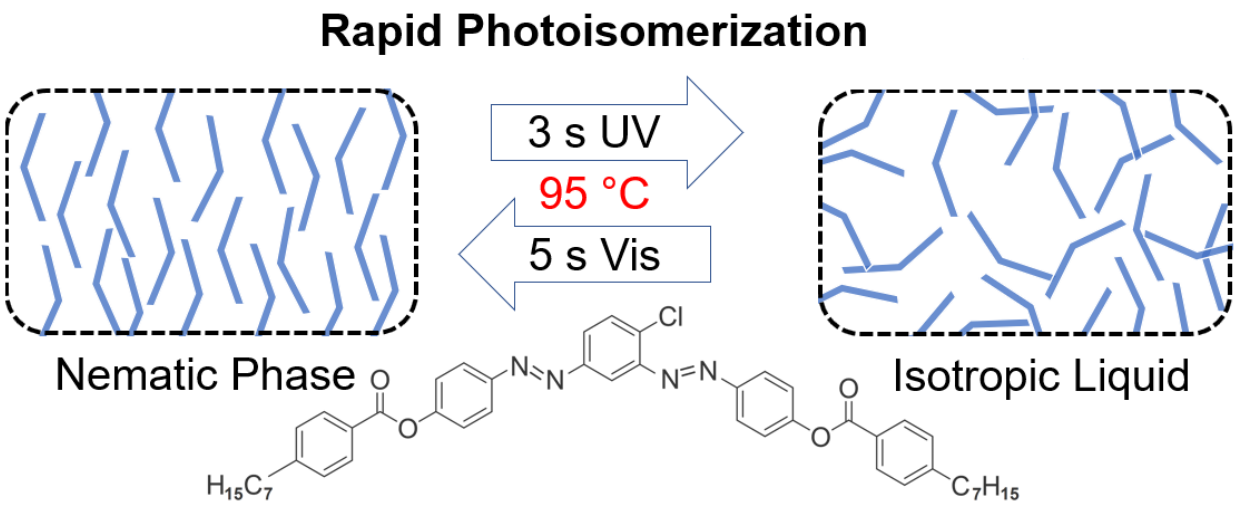

Abstract

Azobenzene-based bent-core liquid crystals demonstrate a variety of mesomorphic behaviors and photochromic properties which are desirable for optical switching. In this study, a series of novel compounds were synthesized by adding azo functional groups and chlorine substituent to the central bent-cores to form a 4-chloro-1,3-dizaophenylene bent-core. Fourier-transform infrared spectroscopy (FTIR), ^{1}H and ^{13}C nuclear magnetic resonance (NMR), mass spectrometry (MS), differential scanning calorimetry (DSC), polarized optical microscopy (POM), and ultraviolet–visible spectroscopy (UV-Vis) were performed to evaluate the structure, mesogenic properties, and photosensitivity of these synthesized compounds. The experimental results show that these compounds exhibit a broad temperature window up to 63.8 °C for nematic phase. In addition, the enhancement of photonic properties of these compounds was exemplified by the high conversion ratio and the rapid rate of *trans – cis* photoisomerization of compound **4c**. The *cis* fraction of **4c** can reach 0.81. At 95 °C, **4c** in nematic phase became isotropic liquid under UV-irradiation in 3 seconds and can be restored to nematic under natural visible light in 5 seconds. At room temperature, **4c** when dissolved in ethyl acetate solution can reach photostationary state in 10 seconds. Quantum mechanics calculation confirms that using azos instead of esters as the central linkages can effectively reduce the molecular dipole moment, which appears to promote favorable mesogenic and photonic characteristics. Moreover, varying the carbon number in the terminal alkyl chains can alter molecular polarity and polarizability, especially the dipole moment and polarizability anisotropy, of which the variations are strongly correlated with the phase transition temperature and temperature range of nematic phase. These findings suggest that 1) changing azo group position can effectively alter the intermolecular interactions by varying molecular polarity and polarizability; 2) reducing long-range electrostatic interactions can promote

favorable mesogenic and possibly photonic properties of azobenzene bent-core liquid crystal. This study linking the mechanistic details with phase behaviors provides a novel approach to improve the material design for photonic technology.

Keywords:

bent-core liquid crystal; 4-chloro-1,3-diazobenzene; synthesis; nematic phase; photoisomerization; molecular modeling; quantum mechanics calculations

1. Introduction

Signal switch is vital to the data transmission in communication and information technology. Photonic technology such as optical fiber has tremendous bandwidth compared to electrical technology because of the significantly weaker interactions between photons than that of electrons.[1] However, current design of optical switch still requires electrical control due to the limitation of materials, which hinders the deployment of photonic technology to a larger scale. Therefore, discovering new phototunable materials is critical to the future design of optical switch.[1–3]

Photosensitive liquid crystals, especially azobenzene-based bent-core liquid crystals (ABLCs), are promising materials for optical switching.[4–7] ABLC compounds can be highly photochromic and mesogenic due to the reversible *trans-cis* photoisomerization of azo group (–N=N–) induced by proper irradiation of ultraviolet or visible light.[8,9] These characteristics also give rise to a myriad of potential applications of ABLC in areas such as elastomer, holographic imaging, optical data storage, and nanomachines.[10–14]

To date, the majority of ABLC compounds implemented at least one ester as the direct linkage of the central bent-core and or deployed azo groups in the distant side arms,[8,15–20] which

usually exhibited high temperatures of phase transition, far above room temperature 25 °C, and narrow temperature ranges of nematic phases. To lower the phase transition temperature and broaden the temperature range of nematic phases, recent studies emphasized on structural alterations such as introducing different lateral substitutions on the bending core,[15,16,21] varying the number of aromatic units,[17,22–24] modifying the type, number, and position of linkage groups,[17,25–29] and changing the type and length of the terminal chains.[17,18,28–31] Yet, the mesogenic phase behaviors of current ABLCs are still unfavorable for practical applications.

We hypothesized that the linking groups adjacent to the central bent-core play a vital role in determining the mesogenic properties of ABLCs. The ester groups commonly used on the central bent-cores as the linking units can induce strong electrostatic forces that contribute to the intermolecular interactions of ABLCs, leading to high phase transition temperatures and narrow nematic phases. Previous studies suggest that the location of azo linkage does not exert significant influence on the mesogenic behavior; if azo bond is close to central ring, it can even inhibit the formation of mesogenic phases.[17,25] However, their conclusions were based on compounds with a single azo linkage. This study proposed an alternative approach to improve the design of ABLC by using two azo bonds instead of esters as the central linkages that connect the central bent-core, which would weaken the intermolecular interactions and therefore enhance the overall performance of ABLC. ABLC compounds synthesized in this study were derived from 4-chloro-1,3-diazobenzene. Each of them possesses two azo linkages and one chlorine substituent in the 1,3-position and 4-position, respectively, at the central aromatic ring and terminal alkyl chains.

2. Materials and methods

2.1 Materials

Anhydrous aluminum trichloride (chemically pure), N, N'-dicyclohexylcarbodiimide (DCC), and 4-dimethylaminopyridine (DMAP) were obtained from Tianjin Fuchen Chemical Reagent (China), Nanjing Chemical Reagent (China), and Xiya Reagent (China), respectively. All chemicals used in this study are of analytical grade, unless otherwise stated. 4-n-hexylbenzoic acid, 4-n-heptylbenzoic acid, 4-n-octylbenzoic acid, 4-n-decylbenzoic acid, and 4-n-decylbenzoic acid were synthesized in our laboratory. Reaction products were purified by silica gel column chromatography and recrystallized three times from ethanol – dichloromethane 1:1 mixture.

2.2 Characterization

Reactions required low temperature were conducted in Zhengzhou Greatwall DHJF-8002 low temperature constant temperature stirring reaction bath. Infrared spectroscopy was performed by a Thermo Nicolet Avatar 330 FTIR. ^{1}H NMR spectra were obtained from a Varian INOVA 400 spectrometer (400 MHz) using tetramethylsilane (TMS) as the reference standard. Differential scanning calorimetry (DSC) experiments were conducted on a TA Instruments DSC Q-20 with a scanning rate of 5 °C/ min and natural cooling. Phase transition and optical textures of liquid crystal compounds were characterized by a polarizing optical microscope (POM) XPN-100E from Shanghai Changfang Optical Instrument.

UV-Visible absorption spectroscopy was collected by a UV-8000S spectrophotometer from Shanghai Metash Instrument. UV-Vis experiments were conducted using a wavelength range from 200 nm to 550 nm and a scan rate of 1 nm/s. UV-Vis spectral data were used i. to measure the isomer fraction by dissolving sample in dilute solution of ethyl acetate (2.5×10^{-5} mol/L) at room temperature and ii. to characterize the UV-induced photoisomerization of mesogenic phases at 95 – 100 °C. The data collection of UV-Vis spectroscopy started when the absorbance value of the two consecutive measurements were identical.

2.3 Synthesis

Compound **4a–4g** were synthesized according to Figure 1, of which the steps are described below.

2.3.1 Synthesis of 4-chloro-1,3-dinitrobenzene **(I)**[32]

Chlorobenzene (40 ml) was added into a 500 ml three-neck flask with magnetic stir bar. The temperature was maintained at 95 °C. Concentrated nitric acid (117.6 ml) and concentrated sulfuric acid (123.6 ml) were added in the flask. The solution mixture was stirred for 5 hours, in which the reaction was monitored by thin layer chromatography (TLC). The reaction product was washed with hot water to reach pH neutral, vacuum-filtered, and air-dried. This step produced yellow crystals.

Yield: 55.07 g, 85.2%, melting point (m.p.) 48 °C. FTIR (KBr, ν_{max}, cm^{-1}): 3082.32 (Ar–H), 1618.15, 1528.35 (Ar), 1474.40, 1352.32, 1306.78, 1202.84, 1102.45.

2.3.2. Synthesis of 4-chlorom-1,3-diaminobenzene **(II)**[33]

pure iron powder (28 g, 0.5 mol), glacial acetic acid (45 g), and 100 mL deionized water were added into a 250 mL three-necked flask. Once the solution was heated to 70 ~ 80 °C, compound (**I**) (20.2 g, 0.1 mol) was added. The reaction was carried out for 4h, which was monitored by TLC to ensure completion. The product mixture was filtered and washed with hot water twice to remove nonpolar impurities. The pH of the filtrate was adjusted to pH 10.0 with saturated Na_2CO_3 solution. The organic phase was extracted with 30 mL ethyl acetate repeated for thrice and then dried with anhydrous K_2CO_3, yielding a crude black product. The product was purified by silica gel column chromatography. This step produced a needle-shaped brown solid of compound (**II**).

Yield: 10.5 g, 74.2%, m.p. 86-88 °C. FTIR (KBr, ν_{max}, cm^{-1}): 3343.37, 3405.11, 3315.06 (N–H), 3211.17 (Ar–H), 1615.53, 1577.97, 1496.67, 1451.98 (Ar), 1333.37, 1274.30, 1208.48, 1147.56, 1106.67, 1044.15, 845.96.

2.3.3 Synthesis of 4-chloro-1,3-bis (4-hydroxyphenyl)azobenzene **(III)**[34]

Chilled concentrated hydrochloric acid (40 mL, 0.5mol) was added in a three-necked flask. The temperature was maintained at below –25 °C. A solution prepared from sodium nitrite (12.5 g, 0.18 mol) and 19 mL deionized water was added dropwise while stirring slowly. Then, a solution prepared from compound (**II)** (7.15g, 0.05mol) and concentrated hydrochloric acid (25mL) was added in multiple steps while gradually increasing the stirring speed. The reaction lasted for 0.5 hour, generating a yellow transparent liquid. Urea pellets (4.8 g, 0.08mol) were added into the liquid dropwise while stirring to yield a diazonium salt.

The diazonium salt was added slowly to a three-necked flask containing a solution of phenol (11.3g, 0.12mol), sodium carbonate (31.8g, 0.3mol) and water (200ml). The mixture in the flask was stirred for 3h in a cold-water bath, of which the reaction was monitored by the TLC. Once the reaction was completed, the mixture was filtered. The resultant filter cake was recrystallized from ethanol. 10.96g of yellow crystals of compound (**III**) was obtained. Yield: 62.3%. m.p. 164 ~ 166 °C. FTIR (KBr, ν_{max}, cm^{-1}): 3333.1 (–OH), 1702.11, 1583.27, 1502.13, 1473.53 (Ar), 1256.44, 1223.10, 1192.22, 1069.13, 1028.42, 853.33; ^{1}H NMR (400 MHz, $CDCl_3$, δ, ppm): 8.31 (s, 1H), 7.95 ~ 7.97 (d, J = 8 Hz, 1H), 7.67 ~ 7.77 (m, 5H), 7.18 ~ 7.21 (t, J = 6 Hz, 4H), 5.08 (s, 2H); ^{13}C NMR (100 MHz, $CDCl_3$): 161.118, 152.732, 149.855, 130.145, 129.282, 124.259, 120.387, 118.365, 115.927. MS m/z (%): 353.65 (65.5, M+1), 231.67 (19.5), 111.67 (13.1).

2.3.4 Synthesis of ABLC compound **4a–4g** [35]

Compound (**II**) (1.66 g, 5mmol), 4-alkylbenzoic acid (10mmol), DCC (12 mmol), DMAP (1.2 mmol) and CH_2Cl_2 (50mL) were added into a 100 mL three-necked flask. The mixture was stirred at room temperature for 24 hours, and the reaction was monitored by TLC. Upon completion, the mixture was filtered and washed with CH_2Cl_2. The solute was extracted by evaporating the solvent under reduced pressure and then purified by silica gel column chromatography.

4-Chloro-1,3-bis(4-((4-pentylphenyl)acyloxy)-1-(E)-azophenyl)benzene **4a**: 2.52g yellow solid flakes, yield: 75.8%. m.p: 103 ~ 104 °C. FTIR (KBr, ν_{max}, cm^{-1}): 2930.13, 2851.70 (-CH_2-), 1680.54, 1643.95, 1613.23, 1546.77, 1507.93, 1447.28 (Ar), 1354.67, 1337.28, 1276.20, 1236.88, 1128.86, 1078.87. ^{1}H NMR (400 MHz, $CDCl_3$): *δ (*ppm): 8.46 (s, ^{1}H), 8.13 ~ 8.15 (d, J = 6 Hz, 4H), 8.05 ~ 8.07 (d, J = 9 Hz, 4H), 7.66 ~ 7.68 (t, J = 7.8 Hz, 1H), 7.39 ~ 7.41 (d, J = 6.5 Hz, 4H), 7.31 ~ 7.33 (d, J = 6.5 Hz, 4H), 2.68 ~ 2.70 (t, J = 4 Hz, 4H), 1.54 ~ 1.64 (m, 4H), 1.30 ~ 1.36 (m, 8H), 0.875 ~ 0.89 (t, J = 6 Hz, 6H). ^{13}C NMR (100 MHz, $CDCl_3$) δ (ppm): 164.929, 153.388, 153.342,150.142, 149.719, 130.365, 129.702, 128.773, 126.640, 125.442, 124.367, 122.531, 116.501, 36.149, 31.935, 31.172, 22.726, 14.171. MS m/z (%): 701.64 (72.5, M+1), 497.62 (13.6), 351.57 (22.3).

4-Chloro-1,3-bis(4-((4-hexylphenyl)acyloxy)-1-(E)-azophenyl)benzene **4b**: 2.45g yellow solid flakes, yield: 7.23g, m.p. 92 ~ 93 °C. FTIR (KBr, ν_{max}, cm^{-1}): 2952.11 (–CH2), 2441.50, 1675.36, 1623.45, 1623.13, 1556.78, 1517.83, 1457.24 (Ar), 1356.69, 1327.18, 1256.10, 1246.82, 1158.86, 998.87. ^{1}H NMR (400 MHz, $CDCl_3$) δ (ppm): 8.55 (s, 1H), 8.21 ~ 8.23 (d, J = 6.5 Hz, 4H), 8.125 ~ 8.15 (d, J = 9 Hz, 4H), 7.84 ~ 7.86 (t, J = 6.5 Hz, 1H), 7.41 ~ 7.43 (d, J = 7.8 Hz, 4H), 7.32 ~ 7.34 (d, J = 6.5 Hz, 4H), 2.70 ~ 2.72 (t, J = 5Hz, 4H), 1.62 ~ 1.65 (m, 4H), 1.31 ~ 1.38

(m, 12H), 0.90 ~ 0.92 (t, J = 6Hz, 6H); ^{13}C NMR (100 MHz, $CDCl_3$) δ (ppm): 164.929, 153.388, 153.342, 150.142, 149.719, 130.365, 129.702, 128.773, 126.640, 125.442, 124.367, 122.531, 116.501, 36.149, 31.935, 31.172, 29.325, 22.726, 14.171. MS m/z (%): 729.53 (55.25, M+1), 587.62 (15.4), 351.54 (20.3).

4-Chloro-1,3-bis(4-((4-heptylphenyl)acyloxy)-1-(E)-azophenyl)benzene **4c**: 2.48g yellow needle crystal, yield: 71.5%, m.p. 84 ~ 85.5 °C. FTIR (KBr, ν_{max}, cm^{-1}): 2918.17, 2849.16 (–CH2), 1169.63, 1645.76, 1613.79, 1542.68, 1507.81, 1450.59 (Ar), 1355.50, 1339.12, 1296.69, 1233.43, 1125.32, 841.01. ^{1}H NMR (400 MHz, $CDCl_3$) δ (ppm): 8.32 (s, 1H), 8.09 ~ 8.11 (d, J = 6.5 Hz, 4H), 7.99 ~ 8.01 (d, J = 8 Hz, 4H), 7.53 ~ 7.55 (t, J = 6.5 Hz, 1H), 7.18 ~ 7.20 (d, J = 8 Hz, 4H), 7.07 ~ 7.09 (d, J = 6.0 Hz, 4H), 2.60 ~ 2.63 (t, J = 6 Hz, 4H), 1.63 ~ 1.66 (m, 4H), 1.31 ~ 1.36 (m, 16H), 0.89 ~ 0.92 (t, J = 6 Hz, 6H). ^{13}C NMR (100 MHz, $CDCl_3$) δ (ppm): 164.819, 152.378, 152.352, 150.212,149.701, 130.321, 129.732, 128.715, 126.590, 125.356, 124.289, 122.425, 116.423, 36.222, 31.852, 31.225, 30.285, 29.285, 22.589, 14.152. MS m/z (%): 757.59 (71.10， M+1), 587.70 (16.5), 295.58 (28.1).

4-Chloro-1,3-bis(4-((4-n-octylphenyl)acyloxy)-1-(E)-azophenyl)benzene **4d**: 2.66g yellow needle crystal, yield: 75.2%, m.p. 76 ~ 77 °C. FTIR (KBr, ν_{max}, cm^{-1}): 2928.13 (–CH2), 2441.70, 1166.54, 1632.95, 1615.23, 1532.77, 1511.93, 1454.28 (Ar), 1348.67, 1342.28, 1286.20, 1228.88, 1138.86, 886.25. ^{1}H NMR (400 MHz, $CDCl_3$) δ (ppm): 8.43 (s, 1H), 8.17 ~ 8.19 (d, J = 6.5 Hz, 4H), 8.03 ~ 8.05 (d, J = 8.8 Hz, 4H), 7.66 ~ 7.68 (t, J = 6.0 Hz, 1H), 7.36 ~ 7.38 (d, J = 5 Hz, 4H), 7.29 ~ 7.31 (d, J = 6 Hz, 4H), 2.68 ~ 2.71 (t, J = 6Hz, 4H), 1.65 ~ 1.68 (m, 4H), 1.32 ~ 1.37 (m, 20H), 0.89 ~ 0.92 (t, J = 6 Hz, 6H). ^{13}C NMR (100MHz, $CDCl_3$) δ (ppm): 164.759, 153.258, 153.452, 150.322, 149.899, 130.425, 129.882, 128.123, 126.540, 125.112, 124.337, 122.441, 116.551, 36.229, 31.985, 31.122, 30.255, 29.852, 29.285, 22.526, 14.151. MS m/z (%):

785.72 (50.45, M+1), 351.60 (11.7), 295.68 (27.4).

4-Chloro-1,3-bis(4-((4-n-nonylphenyl)acyloxy)-1-(E)-azophenyl)benzene **4e**: 2.55 g yellow flake solid, yield: 70.8%, m.p. 73 ~ 74 °C. FTIR (KBr, ν_{max}, cm^{-1}): 2920.13, 2861.70 (–CH2), 1166.54, 1164.97, 1622.32, 1536.67, 1517.83, 1457.32 (Ar), 1344.57, 1347.18, 1266.10, 1246.78, 1340.46, 959.21. ^{1}H NMR (400 MHz, $CDCl_3$) δ (ppm): 8.36 (s, 1H), 8.24 ~ 8.26 (d, J = 6.5 Hz, 4H), 8.08 ~ 8.10 (d, J = 8 Hz, 4H), 7.58 ~ 7.60 (t, J = 4 Hz, 1H), 7.38 ~ 7.40 (d, J = 6.5 Hz, 4H) 7.31 ~ 7.33 (d, J = 6.5 Hz, 4H), 2.77 ~ 2.80 (t, J = 6 Hz, 4H), 1.70 ~ 1.74 (m, 4H), 1.35 ~ 1.41 (m, 24H), 0.88 ~ 0.91 (t, J = 6 Hz, 6H). ^{13}C NMR (100 MHz, $CDCl_3$) δ (ppm): 164.829, 153.348, 153.522, 150.322, 149.889, 130.325, 129.652, 128.553, 126.650, 125.322, 124.427, 122.551, 116.441, 36.259, 31.335, 31.152, 30.255, 30.145, 30.025, 29.255, 22.746, 14.131. MS m/z (%): 813.65 (55.5, M+1), 351.71 (17.6). 203.31 (15.5).

4-Chloro-1,3-bis(4-((4-n-decylphenyl)acyloxy)-1-(E)-azophenyl)benzene **4f**: 2.57g yellow needle crystal, yield: 69.8%. m.p: 65 ~ 66 °C. FTIR (KBr, ν_{max}, cm^{-1}): 2920.01, 2850.68 (–CH2), 1728.64, 1608.83, 15993.34, 1496.65, 1466.78, 1416.72 (Ar), 1266.35, 1209.43, 1174.94, 1145.96, 1066.17, 1017.92. ^{1}H NMR (400 MHz, $CDCl_3$) δ (ppm): 8.46 (s, 1H), 8.14 ~ 8.16 (d, J = 6.4 Hz, 4H), 8.06 ~ 8.08 (d, J = 8 Hz, 4H), 7.68 ~ 7.69 (t, J = 4 Hz, 1H), 7.38 ~ 7.40 (d, J = 8 Hz, 4H), 7.33 ~ 7.34 (d, J = 6 Hz, 4H), 2.70 ~ 2.73 (t, J = 6 Hz, 4H), 1.65 ~ 1.68 (m, 4H), 1.31 ~ 1.35 (m, 28H), 0.90 ~ 0.93 (t, J = 6 Hz, 6H). ^{13}C NMR (100 MHz, CDCl3) δ (ppm): 164.939, 153.378, 153.332, 150.132, 149.729, 130.315, 129.722, 128.783, 126.650, 125.421, 124.363, 122.542, 116.456, 36.222, 31.895, 31.212, 30.225, 30.112, 30.005, 29.855, 29.255, 22.756, 14.161. MS m/z (%): 841.46 (75.10, M+1), 351.66 (22.7), 231.05 (16.8).

4-Chloro-1,3-bis(4-((4-n-dodecylphenyl)acyloxy)-1-(E)-azophenyl)benzene **4g**: 2.72g yellow crystal, yield: 71.2%, m.p. 70.5 ~ 71.5 °C. FTIR (KBr, ν_{max}, cm^{-1}): 2912.13, 2821.70 (–

217 CH_2), 1750.54, 1523.95, 1655.23, 1506.77, 1544.93, 1420.28 (Ar), 1254.67, 1237.28, 1176.20,
218 1136.88, 1028.86, 1001.87. ^{1}H NMR (400 MHz, $CDCl_3$) δ (ppm): 8.46 (s, 1H), 8.13 ~ 8.15 (d, J =
219 6 Hz, 4H), 8.05 ~ 8.08 (d, J = 8.5 Hz, 4H), 7.67 ~ 7.69 (t, J = 4.5 Hz, 1H), 7.39 ~ 7.41 (d, J = 6.5
220 Hz, 4H), 7.32 ~ 7.34 (d, J = 6 Hz, 4H), 2.69 ~ 2.72 (t, J = 6Hz, 4H), 1.64 ~ 1.67 (m, 4H), 1.30 ~
221 1.40 (m, 36H), 0.89 ~ 0.91 (t, J = 6 Hz, 6H). ^{13}C NMR (100 MHz, $CDCl_3$) δ (ppm): 164.929,
222 153.388, 153.342, 150.142, 149.719, 130.365, 129.702, 128.773, 126.640, 125.442, 124.367,
223 122.531, 116.501, 36.149, 31.935, 31.172, 30.855, 30.255, 30.155, 30.022, 29.875, 29.657, 29,285,
224 22.726, 14.171. MS m/z (%): 897.54 (60.5, M+1), 245.31 (23.8), 351.62 (28.3).

225 *2.3.5 Computational Simulations*

226 At the molecular scale, phase transition is the rearrangement of molecules. Phase
227 transitions of nematic liquid crystals are intrinsically associated with the intermolecular
228 interactions especially the long-range non-bonded electrostatic interactions.[36–41] Therefore, it is
229 necessary to examine the molecular polarity that determine the intermolecular electrostatic
230 interactions.[38,42,43] The degree of molecular polarity can be assessed by measuring molecular
231 dipole moment and molecular polarizability.[38,42,43] In this study, computational simulations were
232 performed to determine the molecular properties.

233 Before characterizing the molecular properties, the optimal molecular geometry of each
234 compound needs to be identified at the ground state. Each compound exhibit numerous conformers.
235 For example, compound **4c** contains 104 atoms and 10 rotatable bonds, which generates
236 approximate 60,000 conformers. Apparently, searching conformers of global energy minimum is
237 not viable for computationally demanding simulations especially for those based on quantum
238 mechanics. Therefore, molecular dynamic simulation was applied to screen candidate conformers
239 of global energy minimum. After the screening, quantum mechanics techniques were carried out

on the selected conformers to finalize the geometry optimization. All molecular properties were obtained based on the optimized molecular geometry.

Specifically, molecular dynamics (MD) simulations were conducted by Avogadro 1.2.0, a free cross-platform program. General Amber force field was used due to its specific parameterization for organic molecules.[44–47] Geometry optimization was performed using steepest descent algorithm with a convergence energy of 10^{-7} kcal/mol. Input structural parameters of azobenzene moiety were adopted from previous density functional theory calculation and X-ray diffraction data.[48,49] To find the candidate conformers of the global energy minimum, systematic rotor search was carried out. Semi-empirical (SE) quantum chemistry calculations were performed by MOPAC (Molecular Orbital PACkage, 2016), a general-purpose semi-empirical molecular orbital package free for academic and not-for-profit use, using PM7 Hamiltonian and Baker's EigenFollowing method.[50,51]

To elucidate the dynamics of intermolecular interactions, molecular dipole moment and molecular polarizability were calculated.[52,53] Frequency-dependent dynamic polarizabilities were calculated by time-dependent Hartree-Fock theory.[54] Due to the complexity to express polarizability, here we only compared measurements of polarizability at zero frequency (0 eV) including polarizability isotropic average (α_{iso}) and polarizability anisotropy ($\Delta\alpha$). They can be derived by

$$\alpha_{iso} = \frac{\alpha_{xx} + \alpha_{yy} + \alpha_{zz}}{3}$$

and

$$\Delta\alpha = \sqrt{\frac{(\alpha_{xx} - \alpha_{yy})^2 + (\alpha_{yy} - \alpha_{zz})^2 + (\alpha_{zz} - \alpha_{xx})^2}{2}}$$

where α_{ii} is the principal component of polarizability along the *i*th axis.[53,55,56] The components of dipole moment and polarizability are listed in Table S1 and S2, respectively. In addition, density functional theory (DFT) calculations were deployed to demonstrate that its results are comparable to those of SE (technical details in supplement text). The molecular dipole moments of compounds **4a-4g** calculated by MD, SE, and DFT are compared in Figure S1 and Table S1. Moreover, to compare the experimental results, simulated UV-Vis spectra of **4c** *trans* and *cis* were obtained by DFT as shown in Figure S2, which indicates that the *trans* and *cis* configurations of **4c** are reasonably modelled in our study.

3. Results

3.1 Phases transition temperatures and enthalpies of compounds 4a–4g

The phases, transition temperatures, and transition enthalpies of compounds **4a–4g** are listed in Figure 2 – 3 and Table 1. DSC analysis in Figure 2 shows that while increasing temperature all compounds **4a–4g** displayed an array of phases, including crystalline solid (Cr), smectic (Sm), nematic (N), and isotropic liquid (Iso). The temperatures for Cr – Sm phase transition are ranging from 65.92 °C to 103.37 °C, for Sm – N from 91.36 °C to 124.36 °C, and for N – Iso from 131.26 °C to 162.36 °C. Figure 3 shows that the enthalpies for Cr – Sm, Sm – N, and N – Iso transitions are ranging from 30.3 kJ/mol to 52.3 kJ/mol, 7.4 kJ/mol to 19 kJ/mol, and 2.6 kJ/mol to 4.7 kJ/mol, respectively.

The terminal chain length (carbon number, *n*) demonstrates a pronounced and systematic effect on the phase transition of **4a–4g**. Overall, as the carbon number (n) in the terminal alkyl chains increases, the phase transition temperatures decrease except for the Sm – N transition and transition enthalpies increases except for the N – Iso transition. However, the temperatures of Sm

– N transition initially decreased and then increased as the carbon number increased. The impact from carbon number to the N – Iso transition enthalpies was insubstantial.

Figure 2 shows that generally the phase transition temperatures decrease over the increment of carbon number (*n*) in the terminal alkyl chains. Notably, the phase transition temperatures of N – Iso exhibited a linear relationship with respect to the carbon number, giving a linear fitting with a R^2 (the coefficient of determination) of 0.96. A similar trend was also found for the phase transition of Cr – Sm, which gives a R^2 of 0.96 if treating the data of compound **4g** as an outlier. However, the linear relationship between the Sm – N transition temperatures and the carbon number is insubstantial with a R^2 of 0.01, which indicates the phase behaviors in Sm – N transition are inconsistent with those in the other phase transitions. The only structural difference between compounds **4a–4g** is the length of terminal alkyl chain. Therefore, the inconsistent changes in phase behavior during Sm – N transition could be attributed to the structural difference associated with the terminal chains of compound **4a–4g** during this phase transition.

Additionally, as shown in Figure 2 and Table 1, the liquid crystal phases transition temperature of compound **4a–4g** generally exhibited wide temperature windows of both mesogenic phases ranging from 58.99 °C to 70.68 °C and nematic phases ranging from 19.89 °C to 63.84 °C. In particular, the widest temperature window of mesogenic phase (70.68 °C) and nematic phase (63.84 °C) were both exhibited by compound **4c**, which possessed a moderate length of terminal chains (n = 7). The narrowest temperature window for nematic phase (19.8 °C) was exhibited by compound **4f**, which also exhibited the lowest melting point 65.9 °C.

A previous study showed that the liquid crystal compounds can exhibit a systematic odd-even periodic pattern on phase transition properties according to the carbon number in the terminal alkyl chains.[57–61] Through closer examinations, we noticed that the changes in melting points,

clearing points, and enthalpies exhibit similar odd-even pattern as shown in Figure 2 and 3.

3.2 Molecular dipole moments and polarizability of **4a–4g**

The optimized geometries of **4a–4g** are illustrated in Figure 4, together with their dipole moments. Table 2 list dipole moments (μ), polarizability isotropic average (α_{iso}), and polarizability anisotropies ($\Delta\alpha$) of isomers of **4a–4g**. The μ ranges from 3.7 to 6.1 Debye for *trans* and 4.4 to 9.1 Debye for *cis* isomers, respectively. The α_{iso} ranges from 86.8 to 111.4 Å^3 for trans and 82.9 to 108.4 Å^3 for cis, respectively. The $\Delta\alpha$ ranges from 20.6 to 31.0 Å^3 for *trans* isomers and 9.8 to 18.7 Å^3 for *cis* isomers, respectively. Figure 5 plots the μ, α_{iso}, and $\Delta\alpha$ against the carbon number (n) of the terminal chains, which shows clear trends: i) the variances in molecular dipole between *trans* and *cis* isomers: minimal when n = 7 and maximum when n = 12; ii) increasing carbon number n can linearly increase the α_{iso} for both *trans* and *cis* with the same rate; iii) for *trans*, the increment in n initially reduces the $\Delta\alpha$ when n in the range of 5 to 7 and then gradually increases the $\Delta\alpha$ in the n range of 8 to 12., whereas the *cis* isomers show no clear trend of $\Delta\alpha$.

3.3 Photosensitivity measurement, using **4c** *as an example*

Photosensitivity was measured by UV-Vis spectroscopy. As shown in Figure 6, a series of UV-Vis spectra of **4c** (dissolved in ethyl acetate, room temperature) was collected under the UV irradiation (365 nm, 1 mW/cm^2) for 2 s, 5 s, 10 s, and 30 s. All these spectra exhibited a similar pattern: a strong band and a weak band in the regions of 330 – 340 nm and 430 – 450 nm, respectively. The strong band is attributed by the π–π* transition of the azo unit, which indicates the presence of *trans* isomer, while the weak band is ascribed to the *cis* n–π* transition in cis isomer.[8] As the UV irradiation time prolonged, the intensity of the strong band decreased rapidly, whereas the signal of the weak band gradually increased. This pattern indicates the occurrence of

328 *trans* → *cis* photoisomerization.[8] Interestingly, dissolved **4c** reached photostationary state in 10
329 seconds, significantly faster than reported response rates of similar ABLCs, which are in minutes
330 and even hours.[14,16,17,19–21,25,27,62–65]

331 As shown in Figure 6 (bottom 3 insets), compound **4c** can turn from crystalline solid into
332 nematic phase by heating the pure sample to 95 °C. Under the UV irradiation (365 nm, 1 nW/cm^2),
333 nematic **4c** became isotropic liquid in 3 seconds. Without the UV irradiation, **4c** restored to nematic
334 phase within 5 seconds under indoor natural visible light. These phenomena indicate the presence
335 of reversible *trans* – *cis* photoisomerization. The UV-induced *cis* isomers destabilized the orderly
336 arrangement of *trans* isomers in nematic phase and possibly reduced the phase transition
337 temperatures.[4,27] Under visible light, the backward *trans* ← *cis* photoisomerization started and
338 restored the nematic phase of ***4c***. A video of the phase transitions under POM is available in
339 supplement (POM_UV.mp4).

340 The ratio of the isomer concentrations can be estimated by the following equation:[66,67]

341 $$[cis]_t / [trans]_0 = (1 - A_t / A_0) / (1 - \varepsilon_{cis} / \varepsilon_{trans})$$

342 where $[cis]_t$ is the concentration of *cis* isomer at time *t*, $[\text{trans}]_0$ the initial concentration of *trans*
343 isomer, A_0 and A_t are the absorbances at the wavelength of the same chromophore of sample
344 compound, in which all sample compounds in solution are either *trans* or *cis* isomers, ε_{cis} and ε_{trans}
345 the molar attenuation coefficients (also known as molar extinction coefficient and molar absorption
346 coefficient) of the *cis* and *trans* isomers at a given wavelength of light, respectively.[67]

347 Previous studies on similar azobenzene-based compounds report $\varepsilon_{cis} / \varepsilon_{trans}$ ratios of 0.050,
348 0.053, 0.055, 0.056, and 0.05, corresponding to the UV wavelengths of 320 nm,[67] 325 nm,[67] 355
349 nm,[68] 369.5 nm,[69] and 370 nm,[70] respectively. Therefore, we selected 0.05 as the $\varepsilon_{cis} / \varepsilon_{trans}$ ratio

to estimate the isomer fraction under the irradiation of 365 nm UV. The strong absorption band at 334 nm collected from the 30-second UV irradiation test generated a A_t / A_0 ratio of 0.2348, giving a $[cis]_t$ / $[trans]_0$ ratio of 0.81. This ratio indicates that 81% of nematic **4c** had converted from *trans* to *cis* isomers, which is one of the highest among the reported ratios of similar azobenzene-based compounds.[3,68–73]

4. Discussion

4.1 Effect of azo position

To examining the effect of azo position on ABLC, molecular properties of **4c** and its counterpart **4c-c** using two esters as central linkages were calculated and compared as shown in Figure 7 and Table 3. The comparison shows that the dipole moments of *trans* **4c** (3.85 D) is significantly smaller than that of **4c-c** (6.95 D). The dipole moment of *cis* **4c** (4.11 D) is also noticeably smaller than that of **4c-c** (5.04 D). Interestingly, the DFT calculation shows a larger dipole moment of *cis* **4c** than that of *cis* **4c-c**. Nevertheless, small dipole moment indicates weak electrostatic interactions. Although **4c-c** was not experimentally measured in this study, many ABLC compounds that are structurally similar to **4c-c** were reported in previous studies.[8,17,21,25] These compounds typically exhibited: i) a high temperature threshold to enter nematic phase transition, over 100 °C; 2) a narrow temperature range of nematic phase, usually no more than 20 °C; 3) slow *trans – cis* photoisomerization, which can typically take from a few minutes to even a few hours. Due to the structural resemblance, **4c-c** also likely exhibits these unfavorable traits. Compared to **4c-c, 4c** gained significant improvement on these properties: Sm – N phase transition temperature of 91.4 °C, temperature range of nematic phase 70.7 °C, and rapid photoisomerization within 5 sec. It appears that it is the small dipole moment of **4c** leads to the low phase transition temperature and the wide temperature windows of nematic phase. In addition, the molecular

structures of **4c** isomers prone to form an orderly geometry due to the short terminal chains attaching to the rotatable ester bonds. Therefore, applying azo group as the central linkage to the bent core can lower the phase transition temperature and broaden the temperature windows of mesogenic phases.

Moreover, the polarizabilities of *trans* and *cis* of **4c** are noticeably higher than those of **4c-c**, which corroborates the experimental observations that **4c** is superior to its counterpart **4c-c** in terms of *trans – cis* photoisomerization rates as shown in Table 3. At zero frequency (0 eV), both the α_{iso} and $\Delta\alpha$ of *trans* **4c** (93.6 Å^3 and 20.7 Å^3) are larger than 92.0 Å^3 and 16.5 Å^3 of *trans* **4c-c**, respectively. Since the polarizability α is the first-order response coefficient of molecular polarizability, higher α value typically leads to faster molecular polarization under external electric field.[52] Molecular polarization can drive molecules or molecular groups into favorable orientations, promoting the formation of new phase.[41] The difference in α may also be reflected in phase transition rate. Thus, it is possible that the high polarizability can lead to a rapid phase transition as well as a high *trans – cis* photoisomerization rate as demonstrated by compound **4c**. Further investigation is required to quantify the impact of molecular polarizability on the photosensitivity of this type of compound.

4.2 Effect of molecular polarity and polarizability on phase transition behaviors

Figure 5 (bottom right inset) compares Sm – N transition temperatures and temperature ranges of nematic phase of **4a–4g** compounds with their corresponding dipole moments and polarizability anisotropies. This comparison shows that the impact from terminal chain length to the μ and $\Delta\alpha$ remarkably resembles that of the phase transition temperatures of Sm – N, whereas the effect of terminal chains on the temperature ranges of nematic phase appears to be the opposite. Notably, among these compounds, **4c** with $n = 7$ exhibits extreme values: smallest dipole moment,

the second smallest polarizability anisotropy (20.7 $Å^3$ of 20.6 – 31.0 $Å^3$), the lowest temperature of Sm – N phase transition, and yet the widest temperature range of nematic phase. These patterns show that both molecular polarity and polarizability can indicate the degree of intermolecular interactions in nematic phase, which implies that the nematic phase is the domain of the long-range electrostatic interactions. In addition, an apparent odd-even periodic pattern of dipole moments with respect to the carbon number was observed, which is consistent with our measurements of the phase transition properties.

Figure 4 shows that varying the length of terminal alkyl chains has no apparent impact on the structure of central units with five aromatic rings but causes substantial changes to the structures of terminal alkyl chains. As the carbon number increases, the terminal chains become curly and formed a 'U' shape when the terminal chain has more than nine carbon atoms. This observation suggests that increasing the carbon number can promote the structural disorder of terminal alkyl chains and therefore enhance the molecular dipole moment. Combining the information of μ, $\Delta\alpha$, and the molecular geometry (Figure 4 and 5), it appears that effect of terminal alkyl chain is biphasic. Elongating the alkyl chains can reduce both μ and $\Delta\alpha$ and improve the flexibility of terminal chain structures. However, when the terminal chains were long enough ($n > 7$) that can induce structural disorder, μ and $\Delta\alpha$ would cease to decrease and may even increase as the result of enhanced molecular asymmetry. Therefore, terminal alkyl chain can either enhance or reduce the μ and $\Delta\alpha$ of ABLCs depending on the number of carbon atom, leading to a biphasic effect on the behaviors of nematic phases.

5. Conclusion

To date, this is the first study to synthesize azobenzene-based bent-core liquid crystals (ABLC) using two azo bonds as direct linkages of the central bent-core. A series of 4-chloro-1,3-

diazobenzene bent-core liquid crystal **4a–4g** were synthesized with different length of terminal alkyl chains. These compounds compound exhibited broad temperature windows of nematic phase. In addition, compound **4c** exhibited rapid *trans – cis* photoisomerization in few seconds. Theoretical calculations, such as molecular dynamics (MD) and quantum mechanics (QM) confirmed that when using two azo bonds as the linkage instead of two esters on the central bent-core, the electrostatic interactions are substantially weakened and molecular polarizabilities are enhanced. This finding indicates using azo bonds as central linkages can promote favorable phase behaviors and optical properties. Molecular dipole moments calculated by both MD and QM are strongly correlated with the phase transition behavior such as temperatures of Sm – N phase transition and temperature windows of nematic phase. This correlation suggests that electrostatic interactions are the main contributor of intermolecular interactions, especially in nematic phases. According to the simulation results, the terminal alkyl chains demonstrate a diphasic effect on the molecular dipole due to the structural disorder of overextended alkyl chain, which is consistent with the nematic phase behavior of ABLC.

In summary, this study proposed a novel method to synthesize photosensitive liquid crystal compound and deployed synergistic approach to elucidate material properties. Such efforts are imperative for advancing future design of azobenzene-based bent-core liquid crystals:

1. Using 1,3-diazobenzene as the bent-core can reduce the temperature threshold to enter nematic phase and increase the photoisomerization rate (*trans – cis* photoisomerization in seconds with 80% conversion)
2. Changing carbon number of alkyl chain exerts a biphasic effect on the molecular polarization and phase behavior.
3. Molecular dipole and polarizability anisotropy appear to be strongly correlated with

phase behavior properties. Altering molecular polarization through carbon number of terminal chains is a promising approach to design novel ABLC compounds.

Acknowledgments

This study was supported by National Natural Science Foundation of China under Grants 11074054 and 11374067. DFT calculations in this work used the Extreme Science and Engineering Discovery Environment (XSEDE), which is supported by National Science Foundation grant number ACI-1548562.[74] Specifically, it used the Bridges system, which is supported by NSF award number ACI-1445606, at the Pittsburgh Supercomputing Center (PSC).[75] The computation jobs were submitted through a web-based interface maintained by the Perri Group at Sonoma State University, USA.[76]

Disclosure statement

No potential conflict of interest was reported by the authors.

ORCID

Z. Zhang http://orcid.org/0000-0002-0807-8991

References

(1) *Optical Switching*; El-Bawab, T. S., Ed.; Springer US: Boston, MA, 2006. https://doi.org/10.1007/0-387-29159-8.

(2) De Sio, L.; Ricciardi, L.; Serak, S.; La Deda, M.; Tabiryan, N.; Umeton, C. Photo-Sensitive Liquid Crystals for Optically Controlled Diffraction Gratings. *J. Mater. Chem.* **2012**, *22* (14), 6669. https://doi.org/10.1039/c2jm16077c.

(3) Aronzon, D.; Levy, E. P.; Collings, P. J.; Chanishvili, A.; Chilaya, G.; Petriashvili, G. Trans–Cis Isomerization of an Azoxybenzene Liquid Crystal. *Liquid Crystals* **2007**, *34* (6), 707–718. https://doi.org/10.1080/02678290701267480.

(4) Ikeda, T.; Tsutsumi, O. Optical Switching and Image Storage by Means of Azobenzene Liquid-Crystal Films. *Science* **1995**, *268* (5219), 1873–1875. https://doi.org/10.1126/science.268.5219.1873.

(5) Finkelmann, H.; Nishikawa, E.; Pereira, G. G.; Warner, M. A New Opto-Mechanical Effect in Solids. *Phys. Rev. Lett.* **2001**, *87* (1), 015501. https://doi.org/10.1103/PhysRevLett.87.015501.

(6) Reddy, R. A.; Tschierske, C. Bent-Core Liquid Crystals: Polar Order, Superstructural Chirality and Spontaneous Desymmetrisation in Soft Matter Systems. *J. Mater. Chem.* **2006**, *16* (10), 907–961. https://doi.org/10.1039/B504400F.

(7) Mahimwalla, Z.; Yager, K. G.; Mamiya, J.; Shishido, A.; Priimagi, A.; Barrett, C. J. Azobenzene Photomechanics: Prospects and Potential Applications. *Polym. Bull.* **2012**, *69* (8), 967–1006. https://doi.org/10.1007/s00289-012-0792-0.

(8) Alaasar, M. Azobenzene-Containing Bent-Core Liquid Crystals: An Overview. *Liquid Crystals* **2016**, *43* (13–15), 2208–2243. https://doi.org/10.1080/02678292.2016.1175676.

(9) Merino, E.; Ribagorda, M. Control over Molecular Motion Using the *Cis* – *Trans* Photoisomerization of the Azo Group. *Beilstein J. Org. Chem.* **2012**, *8*, 1071–1090. https://doi.org/10.3762/bjoc.8.119.

(10) Natansohn, A.; Rochon, P. Photoinduced Motions in Azo-Containing Polymers. *Chem. Rev.* **2002**, *102* (11), 4139–4176. https://doi.org/10.1021/cr970155y.

(11) Camacho-Lopez, M.; Finkelmann, H.; Palffy-Muhoray, P.; Shelley, M. Fast Liquid-Crystal Elastomer Swims into the Dark. *Nature Mater* **2004**, *3* (5), 307–310. https://doi.org/10.1038/nmat1118.

(12) Wang, Y.; Li, Q. Light-Driven Chiral Molecular Switches or Motors in Liquid Crystals. *Adv. Mater.* **2012**, *24* (15), 1926–1945. https://doi.org/10.1002/adma.201200241.

(13) Garcia-Amorós, J.; Reig, M.; Castro, M. C. R.; Cuadrado, A.; Raposo, M. M. M.; Velasco, D. Molecular Photo-Oscillators Based on Highly Accelerated Heterocyclic Azo Dyes in Nematic Liquid Crystals. *Chem. Commun.* **2014**, *50* (51), 6704–6706. https://doi.org/10.1039/C4CC01450B.

(14) Sunil, B. N.; Srinatha, M. K.; Shanker, G.; Hegde, G.; Alaasar, M.; Tschierske, C. Effective Tuning of Optical Storage Devices Using Photosensitive Bent-Core Liquid Crystals. *Journal of Molecular Liquids* **2020**, *304*, 112719. https://doi.org/10.1016/j.molliq.2020.112719.

(15) Rahman, M. L.; Asik, J.; Kumar, S.; Tschierske, C. Liquid Crystalline Banana-shaped Monomers Derived from 2,7-naphthalene: Synthesis and Properties. *Liquid Crystals* **2008**, *35* (11), 1263–1270. https://doi.org/10.1080/02678290802513808.

(16) Lutfor, M. R.; Hegde, G.; Kumar, S.; Tschierske, C.; Chigrinov, V. G. Synthesis and Characterization of Bent-Shaped Azobenzene Monomers: Guest–Host Effects in Liquid Crystals with Azo Dyes for Optical Image Storage Devices. *Optical Materials* **2009**, *32* (1), 176–183. https://doi.org/10.1016/j.optmat.2009.07.006.

(17) Nagaveni, N. G.; Raghuvanshi, P.; Roy, A.; Prasad, V. Azo-Functionalised Achiral Bent-Core Liquid Crystalline Materials: Effect of Presence of –N=N– Linkage at Different Locations in the Molecular Architecture. *Liquid Crystals* **2013**, *40* (9), 1238–1254. https://doi.org/10.1080/02678292.2013.805831.

(18) Ghosh, S.; Begum, N.; Turlapati, S.; Roy, S. Kr.; Das, Abhijit. Kr.; Rao, N. V. S. Ferroelectric-like Switching in the Nematic Phase of Four-Ring Bent-Core Liquid Crystals. *J. Mater. Chem. C* **2014**, *2* (3), 425–431. https://doi.org/10.1039/C3TC31800A.

(19) Paterson, D. A.; Xiang, J.; Singh, G.; Walker, R.; Agra-Kooijman, D. M.; Martínez-Felipe, A.; Gao, M.; Storey, J. M. D.; Kumar, S.; Lavrentovich, O. D.; Imrie, C. T. Reversible Isothermal Twist–Bend Nematic–Nematic Phase Transition Driven by the Photoisomerization of an Azobenzene-Based Nonsymmetric Liquid Crystal Dimer. *J. Am. Chem. Soc.* **2016**, *138* (16), 5283–5289. https://doi.org/10.1021/jacs.5b13331.

(20) Alaasar, M.; Poppe, S. Cybotactic Nematic Phases with Wide Ranges in Photoresponsive Polycatenars. *Liquid Crystals* **2019**, 1–11. https://doi.org/10.1080/02678292.2019.1690062.

(21) Alaasar, M.; Prehm, M.; Tschierske, C. Influence of Halogen Substituent on the Mesomorphic Properties of Five-Ring Banana-Shaped Molecules with Azobenzene Wings. *Liquid Crystals* **2013**, *40* (5), 656–668. https://doi.org/10.1080/02678292.2013.767949.

(22) Horčic, M.; Kozmík, V.; Svoboda, J.; Novotná, V.; Pociecha, D. Transformation from a Rod-like to a Hockey-Stick-like and Bent-Shaped Molecule in 3,4′-Disubstituted Azobenzene-Based Mesogens. *J. Mater. Chem. C* **2013**, *1* (45), 7560. https://doi.org/10.1039/c3tc31593b.

(23) Gimeno, N.; Pintre, I.; Martínez-Abadía, M.; Serrano, J. L.; Ros, M. B. Bent-Core Liquid Crystal Phases Promoted by Azo-Containing Molecules: From Monomers to Side-Chain Polymers. *RSC Adv.* **2014**, *4* (38), 19694–19702. https://doi.org/10.1039/C4RA02079K.

(24) Dingemans, T. J.; Murthy, N. S.; Samulski, E. T. Javelin-, Hockey Stick-, and Boomerang-Shaped Liquid Crystals. Structural Variations on *p* -Quinquephenyl †. *J. Phys. Chem. B* **2001**, *105* (37), 8845–8860. https://doi.org/10.1021/jp010869j.

(25) Monika, M.; Prasad, V.; Nagaveni, N. G. Hockey Stick-Shaped Azo Compounds: Effect of Linkage Groups and Their Direction of Linking on Mesomorphic Properties. *Liquid Crystals* **2015**, *42* (10), 1490–1505. https://doi.org/10.1080/02678292.2015.1066889.

(26) Bobrovsky, A.; Shibaev, V.; Hamplová, V.; Bubnov, A.; Novotná, V.; Kašpar, M.; Piryazev, A.; Anokhin, D.; Ivanov, D. Photo-Optical Properties of Amorphous and Crystalline Films of Azobenzene-Containing Photochromes with Bent-Shaped Molecular Structure. *Journal of Photochemistry and Photobiology A: Chemistry* **2016**, *316*, 75–87. https://doi.org/10.1016/j.jphotochem.2015.10.021.

(27) Alaasar, M.; Prehm, M.; Tschierske, C. Helical Nano-Crystallite (HNC) Phases: Chirality Synchronization of Achiral Bent-Core Mesogens in a New Type of Dark Conglomerates. *Chem. Eur. J.* **2016**, *22* (19), 6583–6597. https://doi.org/10.1002/chem.201505016.

(28) Alaasar, M.; Prehm, M.; Brautzsch, M.; Tschierske, C. 4-Methylresorcinol Based Bent-Core Liquid Crystals with Azobenzene Wings – a New Class of Compounds with Dark Conglomerate Phases. *J. Mater. Chem. C* **2014**, *2* (28), 5487–5501. https://doi.org/10.1039/C4TC00533C.

(29) Zhang, X.-X.; Zhang, J.-H.; Cong, Y.-H.; Wang, Q.-L.; Jia, Y.-G. Synthesis, Mesomorphic and Photo-Switching Behaviours of Novel Azobenzene Chiral Liquid Crystals Containing (-)-Menthyl. *Liquid Crystals* **2020**, *47* (9), 1345–1353. https://doi.org/10.1080/02678292.2020.1716275.

(30) Alaasar, M.; Prehm, M.; May, K.; Eremin, A.; Tschierske, C. 4-Cyanoresorcinol-Based Bent-Core Mesogens with Azobenzene Wings: Emergence of Sterically Stabilized Polar Order in Liquid Crystalline Phases. *Adv. Funct. Mater.* **2014**, *24* (12), 1703–1717. https://doi.org/10.1002/adfm.201302295.

(31) Alaasar, M.; Prehm, M.; Brautzsch, M.; Tschierske, C. Dark Conglomerate Phases of Azobenzene Derived Bent-Core Mesogens – Relationships between the Molecular Structure and Mirror Symmetry Breaking in Soft Matter. *Soft Matter* **2014**, *10* (37), 7285–7296. https://doi.org/10.1039/C4SM01255K.

(32) Yi, W.; Cai, C. Highly Efficient Dinitration of Aromatic Compounds in Fluorous Media Using Ytterbium Perfluorooctanesulfonate and Perfluorooctanesulfonic Acid as Catalysts. *Synthetic Communications* **2006**, *36* (20), 2957–2961. https://doi.org/10.1080/00397910600773700.

(33) Meng, G.; Zheng, M.-L.; Zheng, A.-Q.; Wang, M.; Shi, J. The Novel Usage of Thiourea Nitrate in Aryl Nitration. *Chinese Chemical Letters* **2014**, *25* (1), 87–89. https://doi.org/10.1016/j.cclet.2013.09.003.

(34) Hegde, G.; Rajkumar, Y. A.; Mei, G. S.; Mahmood, S.; Mandal, U. K.; Sudhakar, A. A. Photoisomerization Behavior of Photochromic Amide-Based Azobenzene Dyes Exhibiting H-Bonding Effect: Synthesis and Characterization. *Korean J. Chem. Eng.* **2016**, *33* (4), 1480–1488. https://doi.org/10.1007/s11814-015-0259-8.

(35) Mathews, M.; Kang, S.; Kumar, S.; Li, Q. Designing Bent-Core Nematogens towards Biaxial Nematic Liquid

Crystals. *Liquid Crystals* **2011**, *38* (1), 31–40. https://doi.org/10.1080/02678292.2010.524716.
(36) Stroobants, A.; Lekkerkerker, H. N. W.; Odijk, T. Effect of Electrostatic Interaction on the Liquid Crystal Phase Transition in Solutions of Rodlike Polyelectrolytes. *Macromolecules* **1986**, *19* (8), 2232–2238. https://doi.org/10.1021/ma00162a020.
(37) Meier, G.; Saupe, A. Dielectric Relaxation in Nematic Liquid Crystals. *Molecular Crystals* **1966**, *1* (4), 515–525. https://doi.org/10.1080/15421406608083290.
(38) Vertogen, G.; de Jeu, W. H. *Thermotropic Liquid Crystals, Fundamentals*; Goldanskii, V. I., Schäfer, F. P., Toennies, J. P., Series Eds.; Springer Series in Chemical Physics; Springer Berlin Heidelberg: Berlin, Heidelberg, 1988; Vol. 45. https://doi.org/10.1007/978-3-642-83133-1.
(39) Gelbart, W. M. Molecular Theory of Nematic Liquid Crystals. *J. Phys. Chem.* **1982**, *86* (22), 4298–4307. https://doi.org/10.1021/j100219a007.
(40) Singh, S. Phase Transitions in Liquid Crystals. *Physics Reports* **2000**, *324* (2–4), 107–269. https://doi.org/10.1016/S0370-1573(99)00049-6.
(41) Israelachvili, J. N. 6 - Van Der Waals Forces. In *Intermolecular and Surface Forces (Third Edition)*; Israelachvili, J. N., Ed.; Academic Press: San Diego, 2011; pp 107–132. https://doi.org/10.1016/B978-0-12-375182-9.10006-5.
(42) Margenau, H.; Kestner, N. *Theory of Intermolecular Forces*, 2nd ed.; Elsevier, 1969. https://doi.org/10.1016/C2013-0-02436-X.
(43) Stone, A. *The Theory of Intermolecular Forces*, 2nd ed.; Oxford University Press, 2013. https://doi.org/10.1093/acprof:oso/9780199672394.001.0001.
(44) Hanwell, M. D.; Curtis, D. E.; Lonie, D. C.; Vandermeersch, T.; Zurek, E.; Hutchison, G. R. Avogadro: An Advanced Semantic Chemical Editor, Visualization, and Analysis Platform. *J Cheminform* **2012**, *4* (1), 17. https://doi.org/10.1186/1758-2946-4-17.
(45) Wang, J.; Wang, W.; Kollman, P. A.; Case, D. A. Automatic Atom Type and Bond Type Perception in Molecular Mechanical Calculations. *Journal of Molecular Graphics and Modelling* **2006**, *25* (2), 247–260. https://doi.org/10.1016/j.jmgm.2005.12.005.
(46) Wang, J.; Wolf, R. M.; Caldwell, J. W.; Kollman, P. A.; Case, D. A. Development and Testing of a General Amber Force Field. *J. Comput. Chem.* **2004**, *25* (9), 1157–1174. https://doi.org/10.1002/jcc.20035.
(47) *Avogadro: An Open-Source Molecular Builder and Visualization Tool. Version 1.2.0*.
(48) Harada, J.; Ogawa, K.; Tomoda, S. Molecular Motion and Conformational Interconversion of Azobenzenes in Crystals as Studied by X-Ray Diffraction. *Acta Crystallogr B Struct Sci* **1997**, *53* (4), 662–672. https://doi.org/10.1107/S0108768197002772.
(49) Biswas, N.; Umapathy, S. Density Functional Calculations of Structures, Vibrational Frequencies, and Normal Modes of *Trans* - and *Cis* -Azobenzene. *J. Phys. Chem. A* **1997**, *101* (30), 5555–5566. https://doi.org/10.1021/jp970312x.
(50) Stewart, J. J. P. Optimization of Parameters for Semiempirical Methods VI: More Modifications to the NDDO Approximations and Re-Optimization of Parameters. *J Mol Model* **2013**, *19* (1), 1–32. https://doi.org/10.1007/s00894-012-1667-x.
(51) Baker, J. An Algorithm for the Location of Transition States. *J. Comput. Chem.* **1986**, *7* (4), 385–395. https://doi.org/10.1002/jcc.540070402.
(52) Kanis, D. R.; Ratner, M. A.; Marks, T. J. Design and Construction of Molecular Assemblies with Large Second-Order Optical Nonlinearities. Quantum Chemical Aspects. *Chem. Rev.* **1994**, *94* (1), 195–242. https://doi.org/10.1021/cr00025a007.
(53) Ladanyi, B. M.; Liang, Y. Q. Interaction-induced Contributions to Polarizability Anisotropy Relaxation in Polar Liquids. *The Journal of Chemical Physics* **1995**, *103* (15), 6325–6332. https://doi.org/10.1063/1.470413.
(54) Kurtz, H. A.; Stewart, J. J. P.; Dieter, K. M. Calculation of the Nonlinear Optical Properties of Molecules. *J. Comput. Chem.* **1990**, *11* (1), 82–87. https://doi.org/10.1002/jcc.540110110.
(55) Skaf, M. S.; Vechi, S. M. Polarizability Anisotropy Relaxation in Pure and Aqueous Dimethylsulfoxide. *The Journal of Chemical Physics* **2003**, *119* (4), 2181–2187. https://doi.org/10.1063/1.1583677.

(56) Smith, S. M.; Markevitch, A. N.; Romanov, D. A.; Li, X.; Levis, R. J.; Schlegel, H. B. Static and Dynamic Polarizabilities of Conjugated Molecules and Their Cations. *J. Phys. Chem. A* **2004**, *108* (50), 11063–11072. https://doi.org/10.1021/jp048864k.
(57) Henderson, P. A.; Seddon, J. M.; Imrie, C. T. Methylene- and Ether-linked Liquid Crystal Dimers II. Effects of Mesogenic Linking Unit and Terminal Chain Length. *Liquid Crystals* **2005**, *32* (11–12), 1499–1513. https://doi.org/10.1080/02678290500284983.
(58) Henderson, P. A.; Niemeyer, O.; Imrie, C. T. Methylene-Linked Liquid Crystal Dimers. *Liquid Crystals* **2001**, *28* (3), 463–472. https://doi.org/10.1080/02678290010007558.
(59) Tschierske, C. Development of Structural Complexity by Liquid-Crystal Self-Assembly. *Angew. Chem. Int. Ed.* **2013**, *52* (34), 8828–8878. https://doi.org/10.1002/anie.201300872.
(60) Neubert, M. E.; Carlino, L. T.; Fishel, D. L.; D'sidocky, R. M. The Effect of Terminal Alkyl Chain Length on Mesomorphic Properties of 4-Alkoxyphenyl-4'-Alkylbenzoates. *Molecular Crystals and Liquid Crystals* **1980**, *59* (3–4), 253–272. https://doi.org/10.1080/00268948008071427.
(61) Inglot, K.; Martyński, T.; Bauman, D. Influence of the Alkyl Chain Length of Some Mesogenic Molecules on Their Langmuir Film Formation Ability. *Liquid Crystals* **2006**, *33* (7), 855–864. https://doi.org/10.1080/02678290600733798.
(62) Choi, S.-W.; Izumi, T.; Hoshino, Y.; Takanishi, Y.; Ishikawa, K.; Watanabe, J.; Takezoe, H. Circular-Polarization-Induced Enantiomeric Excess in Liquid Crystals of an Achiral, Bent-Shaped Mesogen. *Angew. Chem. Int. Ed.* **2006**, *45* (9), 1382–1385. https://doi.org/10.1002/anie.200503767.
(63) Vera, F.; Tejedor, R. M.; Romero, P.; Barberá, J.; Ros, M. B.; Serrano, J. L.; Sierra, T. Light-Driven Supramolecular Chirality in Propeller-Like Hydrogen-Bonded Complexes That Show Columnar Mesomorphism. *Angew. Chem. Int. Ed.* **2007**, *46* (11), 1873–1877. https://doi.org/10.1002/anie.200603796.
(64) Mathews, M.; Zola, R. S.; Yang, D.; Li, Q. Thermally, Photochemically and Electrically Switchable Reflection Colors from Self-Organized Chiral Bent-Core Liquid Crystals. *J. Mater. Chem.* **2011**, *21* (7), 2098–2103. https://doi.org/10.1039/C0JM03479G.
(65) Senyuk, B.; Wonderly, H.; Mathews, M.; Li, Q.; Shiyanovskii, S. V.; Lavrentovich, O. D. Surface Alignment, Anchoring Transitions, Optical Properties, and Topological Defects in the Nematic Phase of Thermotropic Bent-Core Liquid Crystal A131. *Phys. Rev. E* **2010**, *82* (4), 041711. https://doi.org/10.1103/PhysRevE.82.041711.
(66) Fischer, E. Calculation of Photostationary States in Systems A .Dblarw. B When Only A Is Known. *J. Phys. Chem.* **1967**, *71* (11), 3704–3706. https://doi.org/10.1021/j100870a063.
(67) Victor, J. G.; Torkelson, J. M. On Measuring the Distribution of Local Free Volume in Glassy Polymers by Photochromic and Fluorescence Techniques. *Macromolecules* **1987**, *20* (9), 2241–2250. https://doi.org/10.1021/ma00175a032.
(68) Morishima, Y.; Tsuji, M.; Kamachi, M.; Hatada, K. Photochromic Isomerization of Azobenzene Moieties Compartmentalized in Hydrophobic Microdomains in a Microphase Structure of Amphiphilic Polyelectrolytes. *Macromolecules* **1992**, *25* (17), 4406–4410. https://doi.org/10.1021/ma00043a025.
(69) Sasaki, T.; Ikeda, T.; Ichimura, K. Photoisomerization and Thermal Isomerization Behavior of Azobenzene Derivatives in Liquid-Crystalline Polymer Matrixes. *Macromolecules* **1993**, *26* (1), 151–154. https://doi.org/10.1021/ma00053a023.
(70) Wang, W.; Wang, M.-Z. Effect of α-Cyclodextrin on the Photoisomerization of Azobenzene Functionalized Hydroxypropyl Methylcellulose in Aqueous Solution. *Polym. Bull.* **2007**, *59* (4), 537–544. https://doi.org/10.1007/s00289-007-0789-2.
(71) Ya, Q.; Dong, X.-Z.; Chen, W.-Q.; Duan, X.-M. The Synthesis of Aminoazobenzenes and the Effect of Intermolecular Hydrogen Bonding on Their Photoisomerization. *Dyes and Pigments* **2008**, *79* (2), 159–165. https://doi.org/10.1016/j.dyepig.2008.02.004.
(72) Fischer, E. Temperature Dependence of Photoisomerization Equilibria. Part I. Azobenzene and the Azonaphthalenes. *J. Am. Chem. Soc.* **1960**, *82* (13), 3249–3252. https://doi.org/10.1021/ja01498a005.
(73) Naito, T.; Horie, K.; Mita, I. Photochemistry in Polymer Solids. 11. The Effects of the Size of Reaction

Groups and the Mode of Photoisomerization on Photochromic Reactions in Polycarbonate Film. *Macromolecules* **1991**, *24* (10), 2907–2911. https://doi.org/10.1021/ma00010a042.

(74) Towns, J.; Cockerill, T.; Dahan, M.; Foster, I.; Gaither, K.; Grimshaw, A.; Hazlewood, V.; Lathrop, S.; Lifka, D.; Peterson, G. D.; Roskies, R.; Scott, J. R.; Wilkins-Diehr, N. XSEDE: Accelerating Scientific Discovery. *Comput. Sci. Eng.* **2014**, *16* (5), 62–74. https://doi.org/10.1109/MCSE.2014.80.

(75) Nystrom, N. A.; Levine, M. J.; Roskies, R. Z.; Scott, J. R. Bridges: A Uniquely Flexible HPC Resource for New Communities and Data Analytics. In *Proceedings of the 2015 XSEDE Conference on Scientific Advancements Enabled by Enhanced Cyberinfrastructure - XSEDE '15*; ACM Press: St. Louis, Missouri, 2015; pp 1–8. https://doi.org/10.1145/2792745.2792775.

(76) Perri, M. J.; Weber, S. H. Web-Based Job Submission Interface for the GAMESS Computational Chemistry Program. *J. Chem. Educ.* **2014**, *91* (12), 2206–2208. https://doi.org/10.1021/ed5004228.

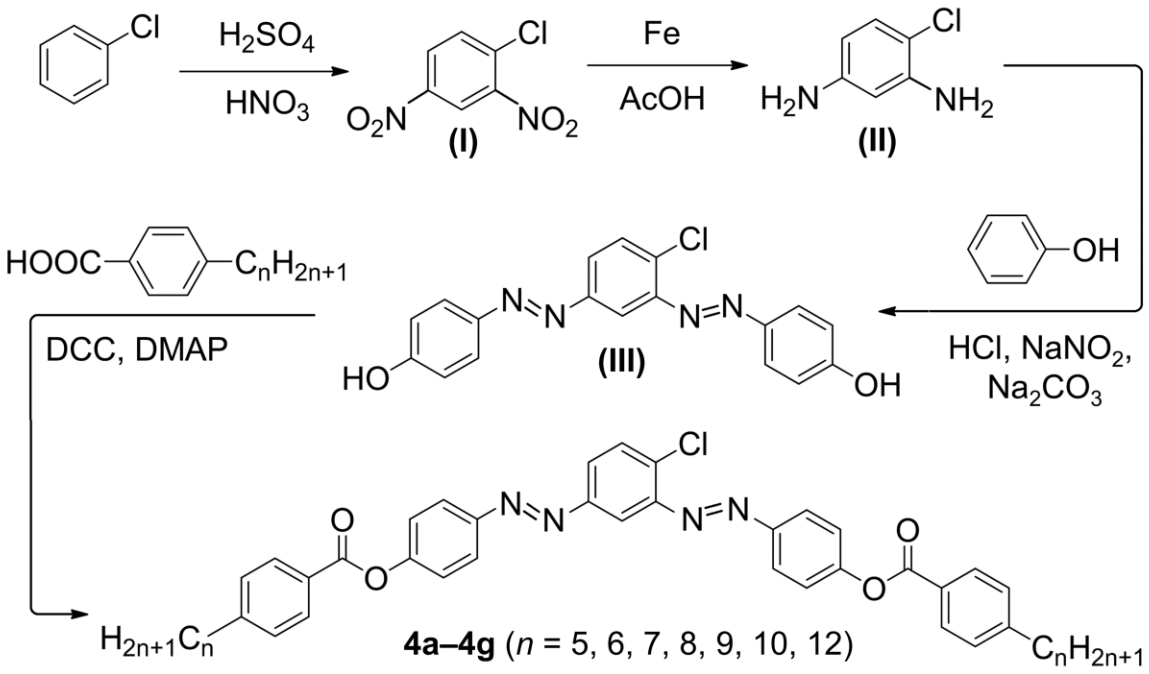

Figure 1. Synthesis of 4-chloro-1,3-diazobenzene bent-core liquid crystals **4a–4g**. "*n*" denotes the number of carbon atoms in the terminal alkyl chains.

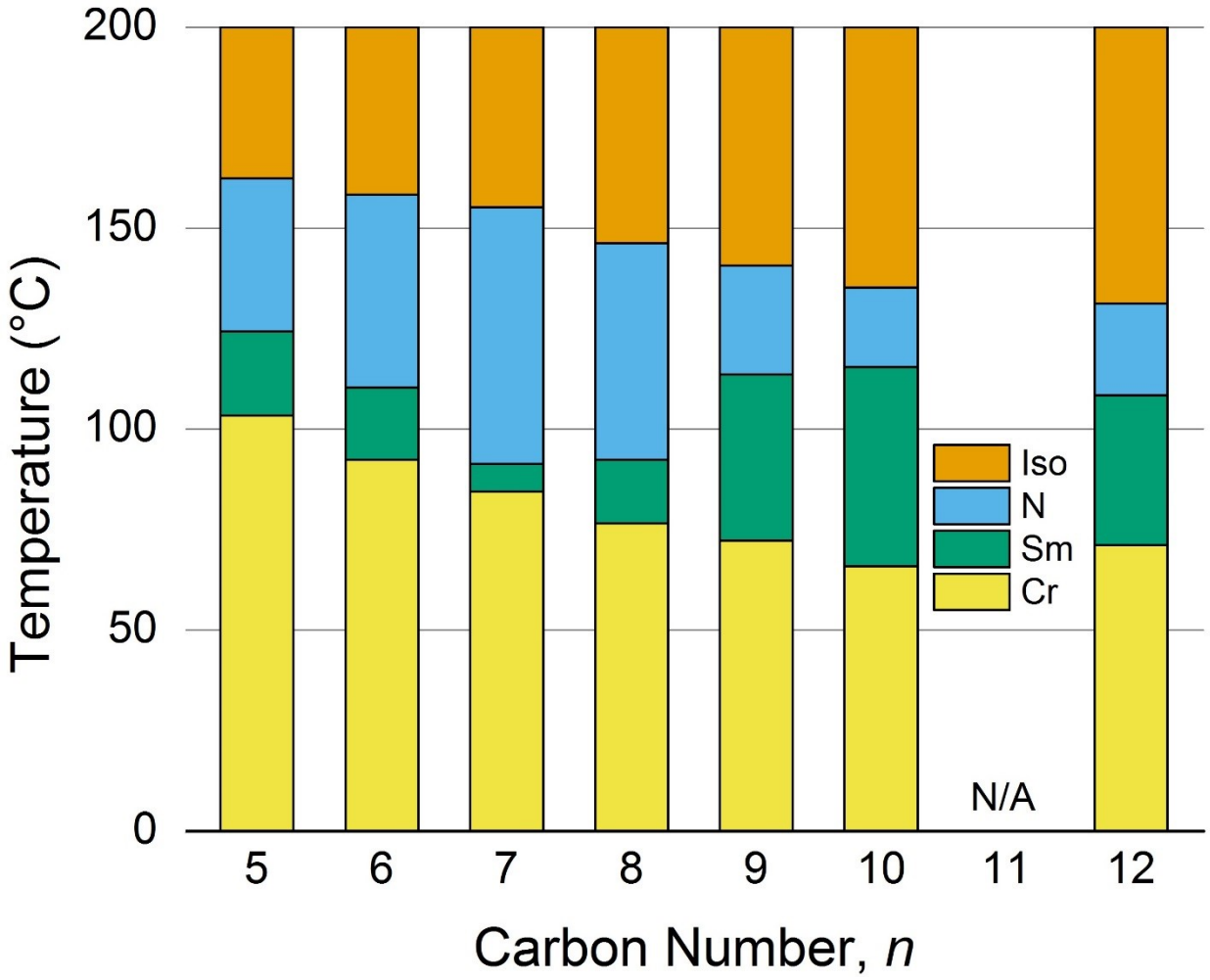

Figure 2. Phase transition temperatures of compounds **4a–4g**. Yellow, pink, cyan, and grey blocks represent crystalline (Cr) solid, smectic (Sm) phase, nematic (N) phase, and isotropic (Iso) phase, respectively.

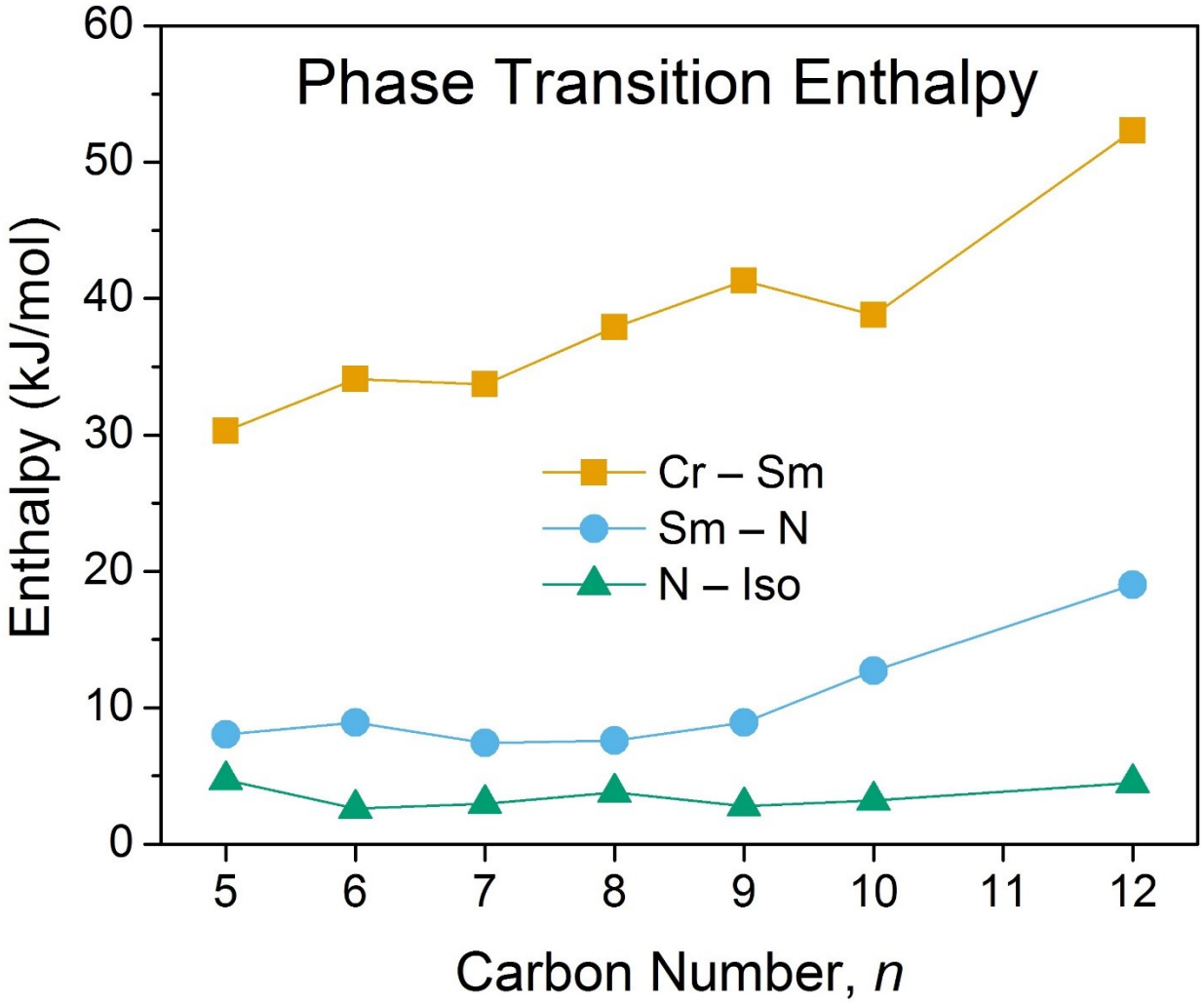

Figure 3. Enthalpies for the phase transitions of compounds **4a–4g**.

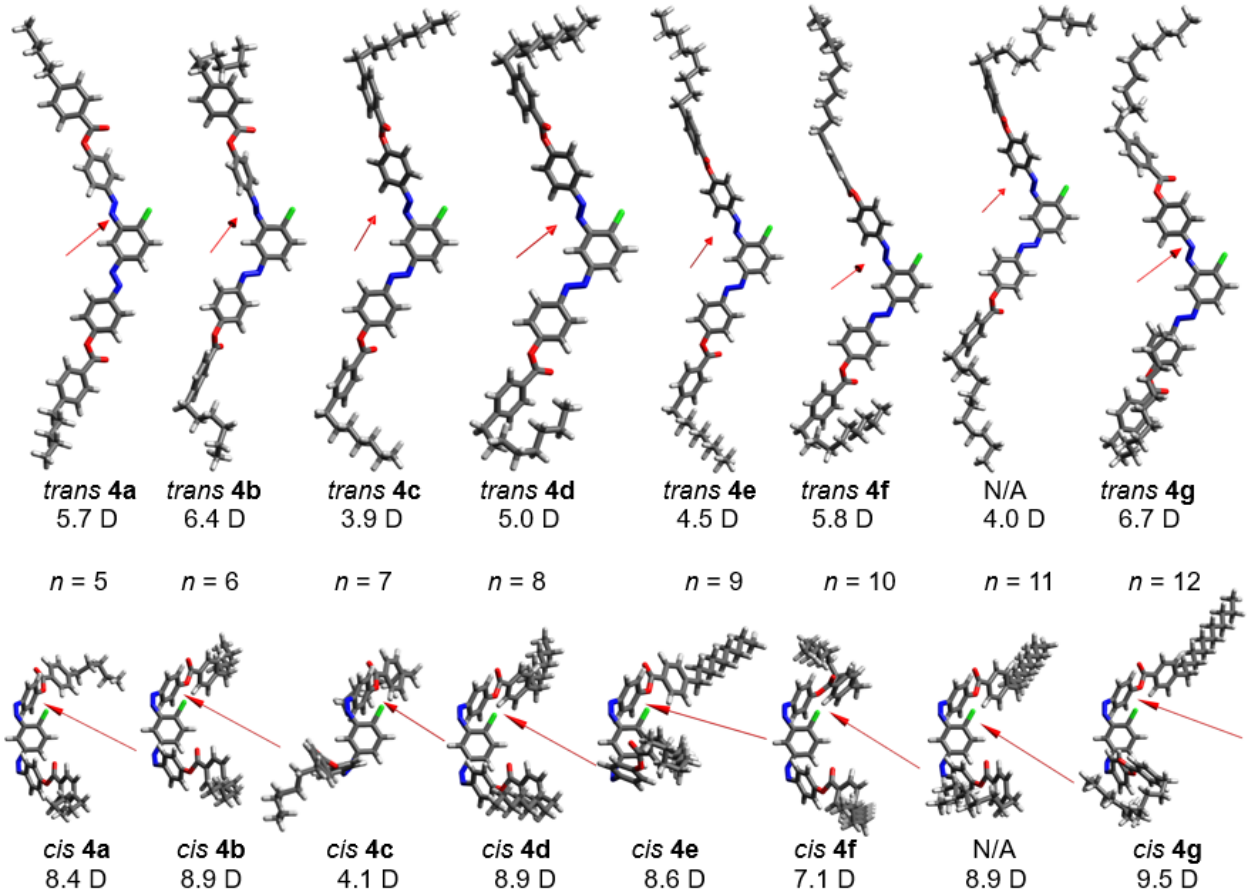

Figure 4. Molecular structures and dipole orientations of *trans* and *cis* isomers of **4a**–**4g** in the ground states. The orientations of dipole moment for each type of isomers are generally consistent. The main structural variation within each isomer group is the spatial arrangement of terminal chain. Please note that N/A refers to the compound with n = 11, which is not synthesized in this study. The molecular dipoles were calculated by MOPAC (D: Debye).

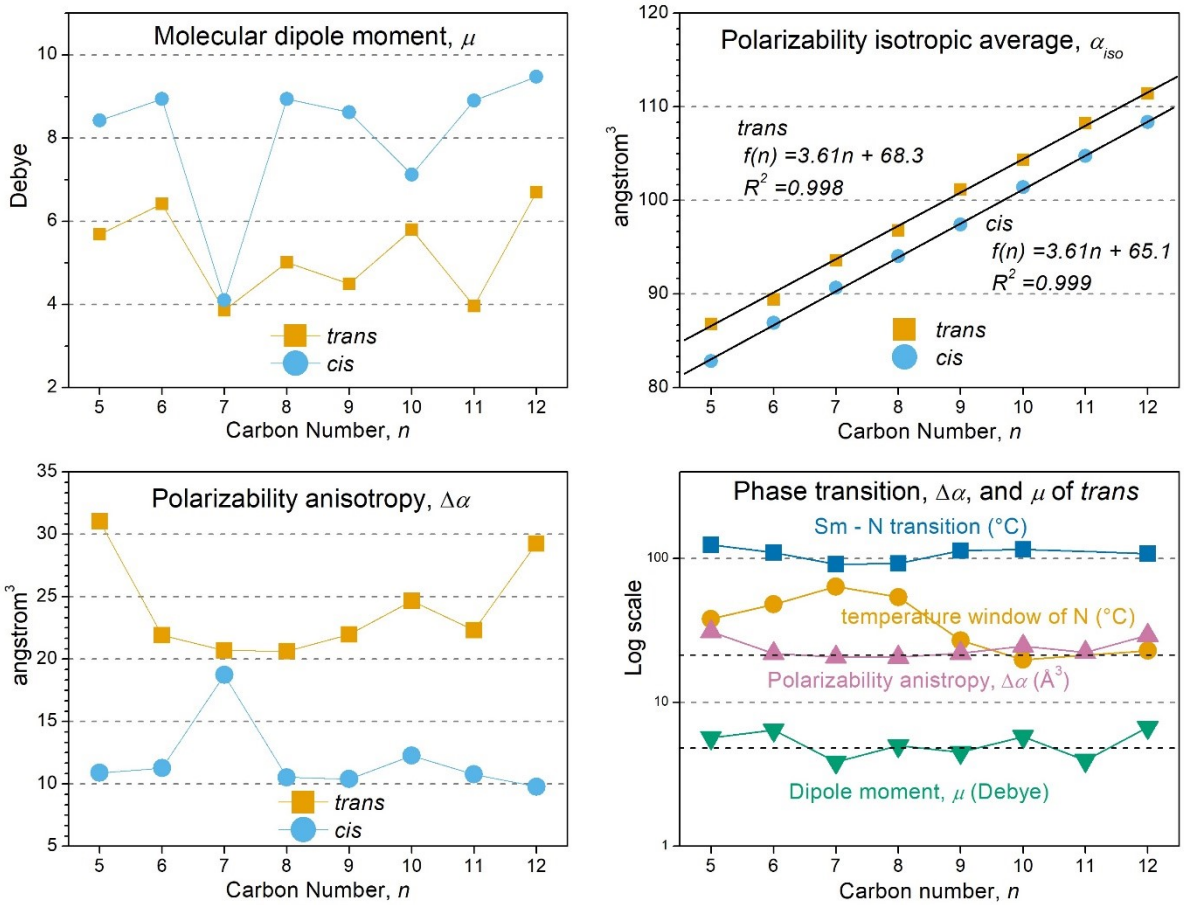

Figure 5. Molecular properties of **4a–4g** and their correlation with the Sm – N transition temperature of **4a–4g**. Top left: molecular dipole moments; top right: polarizability; bottom left: polarizability anisotropies; bottom right: comparison between the Sm – N phase transition temperatures, temperature window of nematic phase, polarizability anisotropies, and dipole moments of *trans* isomers of **4a–4g**.

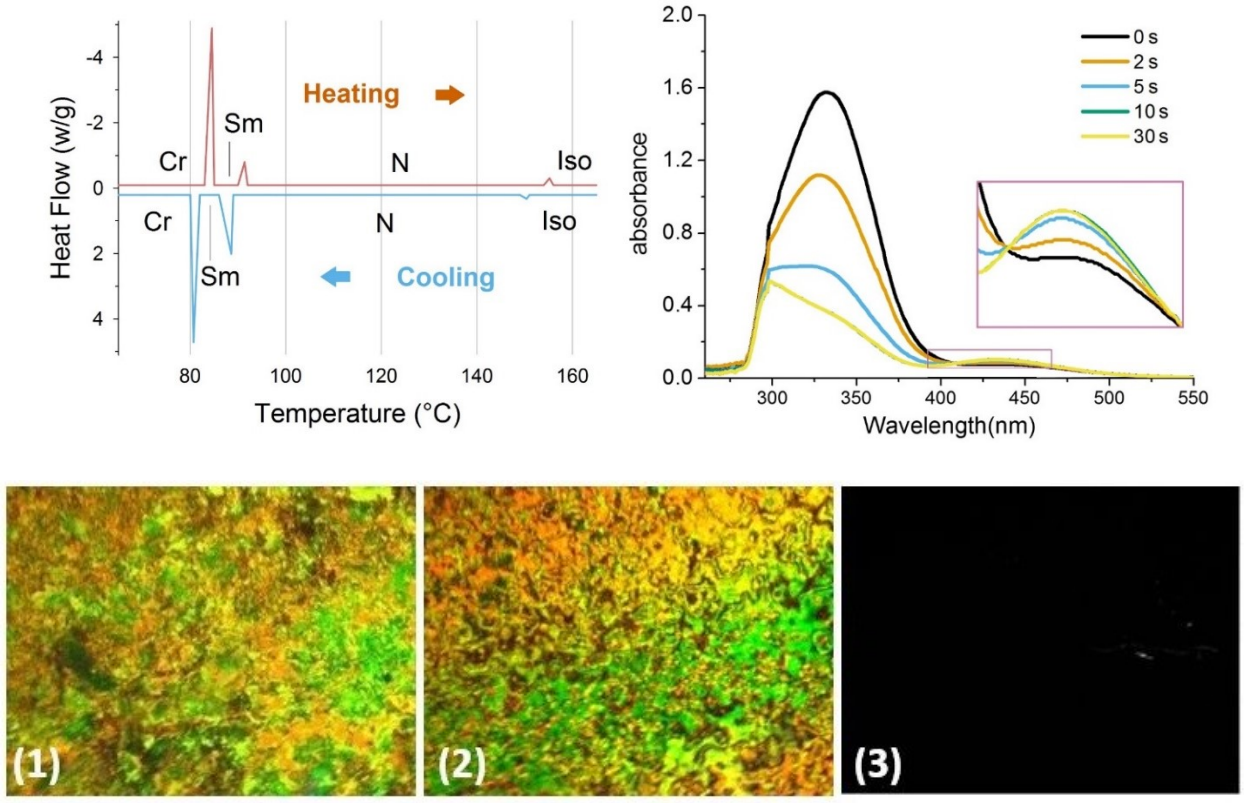

Figure 6. Top left: DSC heating and cooling traces of compound **4c**. Top right: UV-Vis spectra of dissolved compound **4c** under 365 nm UV irradiation for 0 s, 2 s, 5 s, 10 s, and 30 s. Bottom 3 insets**:** polarized optical micrograms of compound **4c** under various conditions: (1) smectic textures at 88 °C, (2) nematic textures at 120 °C, and (3) isotropic liquid phase at 155 °C.

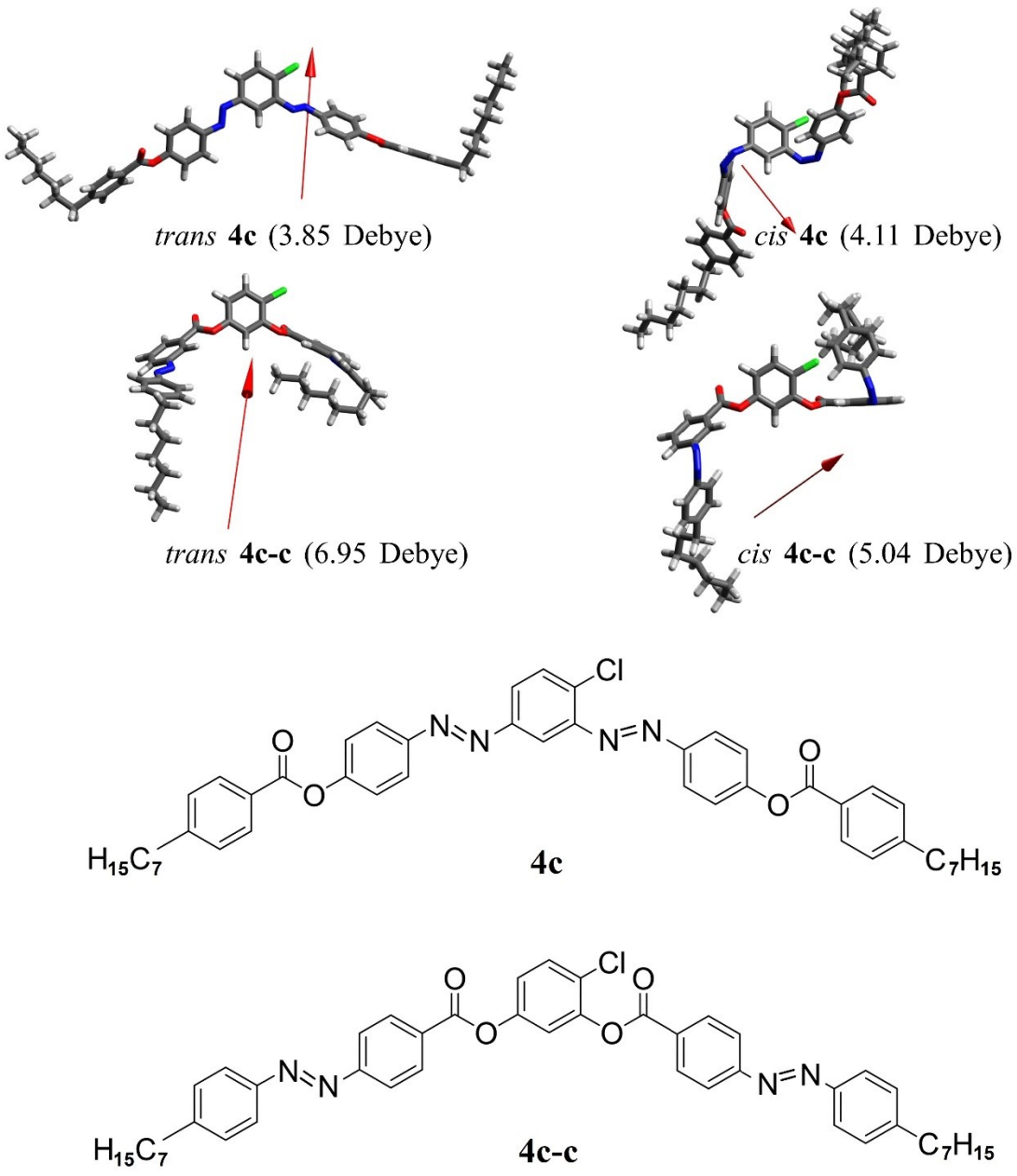

699

700 Figure 7. Top four insets: molecular structures and dipole moments of isomers of compound **4c**

701 and its counterpart **4c-c** at the ground states. Red arrows represent the direction of dipole moment.

702 Bottom two insets: chemical structures of compound **4c** and **4c-c**.

703

Table 1. Phase transition temperatures of compound **4a**–**4g**. "*n*" denotes the carbon number in the terminal alkyl chain; "Cr" the crystalline phase; "Sm" the smectic phase; "N" the nematic phase; "I" the isotropic liquid; "T" the phase transition temperature in °C; "△H" the reaction enthalpy in kJ/mol; "ΔT_{LC}" the temperature window of liquid crystal phase in °C; "ΔT_N" the temperature window of nematic phase in °C ($\Delta T_N = T_{N–I} – T_{Sm–N}$).

Compound	*n*	Phase transition in ℃ [△H, kJ/mol]	ΔT_{LC} (°C)	ΔT_N (°C)
4a	5	Cr 103.37 [30.3] Sm 124.36 [8.05] N 162.36 [4.7] I	58.99	38.00
4b	6	Cr 92.38 [34.1] Sm 110.36 [8.9] N 158.36 [2.6] I	65.98	48.00
4c	7	Cr 84.52 [33.7] Sm 91.36 [7.4] N 155.20 [2.95] I	70.68	63.84
4d	8	Cr 76.56 [37.9] Sm 92.35 [7.6] N 146.23 [3.8] I	69.67	53.88
4e	9	Cr 72.35 [41.3] Sm 113.65 [8.9] N 140.62 [2.8] I	68.27	26.97
4f	10	Cr 65.92 [38.8] Sm 115.46 [12.7] N 135.26 [3.2] I	69.34	19.80
4g	12	Cr 71.20 [52.3] Sm 108.36 [19.0] N 131.26 [4.5] I	60.06	22.90

Table 2. Molecular dipole moments (μ), polarizabilities (α), and polarizability anisotropies ($\Delta\alpha$) of compound **4a–4g** calculated by MOPAC. "*n*" denotes the number of carbon atoms in each terminal alkyl chain.

Compound	*n*	*trans*			*cis*		
		μ (D)	α (Å^3)	$\Delta\alpha$ (Å^3)	μ (D)	α (Å^3)	$\Delta\alpha$ (Å^3)
4a	5	5.689	86.8	31.0	8.424	82.9	10.9
4b	6	6.419	89.4	21.9	8.938	86.9	11.3
4c	7	3.854	93.6	20.7	4.107	90.7	18.7
4d	8	5.010	96.8	20.6	8.937	94.0	10.5
4e	9	4.498	101.2	22.0	8.618	97.4	10.4
4f	10	5.795	104.3	24.7	7.119	101.4	12.3
N/A	11	3.964	108.3	22.3	8.905	104.8	10.8
4g	12	6.700	111.4	29.2	9.472	108.4	9.8

715 Table 3. Comparison of molecular properties between **4c** and its diester counterpart **4c-c.**

	μ (Debye)	α (Å^3)	$\Delta\alpha$ (Å^3)	μ (Debye, DFT)
trans **4c**	3.854	93.6	20.7	3.733155
trans **4c-c**	6.951	92.0	16.5	6.562452
cis **4c**	4.107	90.7	18.7	4.028691
cis **4c-c**	5.038	89.0	7.5	3.499278

716

717